3B2v8.06a/w (Dec 5 2003).51c XML:ver:5.0.1 | IE : 1202 | Prod.Type:FTP pp.1–14(col.fig.:1,7,8) | ED:MangalaGowri PAGN:gopal SCAN:mangala

ARTICLE IN PRESS

Available online at www.sciencedirect.com

SCIENCE DIRECT®

ELSEVIER

International Journal of Impact Engineering ■ (■■■■) ■■■–■■■

INTERNATIONAL JOURNAL OF IMPACT ENGINEERING

www.elsevier.com/locate/ijimpeng

Modelling crimp in woven fabrics subjected to ballistic impact

V.B.C. Tan*, V.P.W. Shim, X. Zeng

Impact Mechanics Laboratory, Department of Mechanical Engineering, National University of Singapore, 9 Engineering Drive 1, Singapore 117576

Received 20 September 2004; received in revised form 24 June 2005; accepted 25 June 2005

Abstract

Woven fabrics are widely used in flexible armour systems for protection against fragments and projectiles from small arms. The woven architecture introduces crimp or undulations in the yarns as they pass alternately over and under orthogonal yarns. An undesirable effect of crimp is excessive deflection in fabric armour during impact. The numerical results of ballistic impact and perforation of woven aramid fabric are presented in this paper. The fabric is modelled as a network of nodal masses connected by one-dimensional viscoelastic elements. The focus of the computational simulation is to compare two different ways of incorporating yarn crimp into the fabric model. Tensile tests on strips of the woven fabric show an initial toe region in the load–deflection curve before the curve asymptotically converges to an approximately straight line beyond a certain strain. The first method of introducing crimp into the fabric model is to include the toe region of the load–deflection curve in the constitutive equation describing the viscoelastic elements. The second method to account for crimp is to physically reflect the woven architecture in the fabric model by arranging the chain of linear elements that define each yarn in a zigzag manner.

Keywords: Woven fabric; Crimp; Ballistic impact; Numerical simulation

*Corresponding author. Tel.: +65 6874 8088; fax: +65 6779 1459.
E-mail address: mpetanbc@nus.edu.sg (V.B.C. Tan).

0734-743X/$ - see front matter © 2005 Published by Elsevier Ltd.
doi:10.1016/j.ijimpeng.2005.06.008

1. Introduction

Woven fabrics constructed from high-strength polymeric fibres are widely used in flexible personal protection systems. They are also effective for the containment of high-speed fragments or munitions to shield critical components in aircrafts and vehicles. Improvements in the ballistic resistance of high-strength fabric armour systems have largely been due to advances in the production of stronger fibres. There are now many polymeric fibres with exceptionally high stiffness and high strength to weight ratios. Examples of materials that are commercially available include aramids (eg. Kevlar®, Twaron®), ultra high molecular weight polyethylene (eg. Spectra®, Dacron®), PBO fibres (e.g. Zylon®) and PIPD fibres (also known as M5®). In addition to the mechanical properties of the fibres, it is reported that the energy absorption capability of fabric armour also depends on its weave architecture, number of fabric plies, areal density and surface treatment of yarns. The ballistic resistance of a fabric is also a function of factors not related to the properties of the fabric, such as impact velocity, impact angle, projectile shape, boundary conditions, etc. A number of studies have been carried out to characterize the ballistic performance of fabrics and to identify key parameters that affect their impact resistance. A comprehensive review of recent research into fabric armour has been reported by Cheeseman and Bogetti [1]. They also presented a detailed description of factors affecting their performance.

The effects of yarn crimp on the impact response of woven fabric are presented in this paper. Crimping in yarns is a distinct characteristic of woven fabrics and has been identified to have an important effect on fabric response to impact loading. When a projectile strikes a fabric, the initial stage of fabric deformation simply causes crimped yarns to straighten. Minimal resistance is presented to the projectile. The fabric only starts to resist the projectile when the yarns have straightened and begin to stretch. Crimp can give rise to excessive transverse deflection and consequently increase blunt trauma.

Ballistic fabrics normally have different levels of crimp in warp and weft yarns because of the weaving process, resulting in weft yarns having lower levels of crimp than warp yarns. This is believed to cause weft yarns to break preferentially to warp yarns during ballistic impacts. To mitigate this phenomenon, Chitrangad [2] proposed a hybrid fabric using fibres with higher failure strain in weft yarns than warp yarns to delay the breakage of weft yarns. New generation fabrics for ballistics applications are now manufactured with equal crimp in weft and warp yarns so that yarns in both directions are loaded equally during projectile impacts. This has resulted in better energy absorption capability.

Apart from actual ballistic tests, computational simulation has also contributed significantly to a better understanding of the mechanisms involved in the impact and perforation process. Yarn crimp is normally included in computational models of fabric because its effects are not negligible. In the current study, two different ways of representing yarn crimp in numerical models of woven fabric are presented and the results obtained from the two methods are compared.

2. Twaron CT716

Ballistic tests were conducted on a plain woven fabric (Tawron® CT716) to evaluate the accuracy of the fabric models. CT716 is made from aramid fibres and its properties are given in

Table 1
Twaron® fabric CT716 specification

Specific density	1.44 g/cm^3
Linear density warp & weft	1100 f 1000 dtex
Areal density	280 g/m^2
Thickness	0.40 mm

Table 1. Twaron CT716 has different degrees of crimp in warp and weft yarns. In standard terminology relating to textiles (ASTM D 123-03), 'warp' refers to yarns in a woven fabric that run lengthwise and parallel to the selvage and 'weft' refers to yarns that run widthwise, i.e., from selvage to selvage. In plain-woven fabrics, weft yarns, also known as fill yarns, are interwoven at right angles into the warp yarns. During the weaving process, weft yarns are normally woven into the fabric with higher tension than the warp yarns. This gives rise to fewer undulations in weft yarns compared to warp yarns. CT716 has a high areal density because of its tight weave. Fig. 1 shows that yarns removed from the fabric retain a significant level of crimping because of the tight weave.

The degree of crimp, as defined by ISO 7211-3, is given by $k = \left[(P-L)/L\right] \times 100\%$, where L is the distance between two ends of the projection of a yarn onto the plane of the fabric and P is the actual length of the yarn. By this definition, warp yarns of CT716 have a crimp of 6.5% and weft yarns 0.99%. The large difference in the levels of crimp suggests a significant difference in the tension of warp and weft yarns during the weaving process.

CT716 fabric has a thickness of 0.398 mm with 123 yarns per 10 cm in the warp direction and 120 yarns per 10 cm in the weft direction. From these data, two crimp parameters, namely, crimp wavelength ($2D$) and crimp amplitude (T), can be determined. The degree of crimp can also be estimated by idealising the yarns as short straight segments connected together in a zigzag arrangement as shown in Fig. 2.

3. Computational model of woven fabric

Several different approaches to modelling woven fabric have been reported. The simplest model assumes the fabric behaves like a membrane [3,4]. The various membrane models vary in complexity depending on the constitutive model selected for the membrane material. Neglecting the strain-rate dependency of polymeric yarns may lead to underestimation of the ballistic limit of the fabric, while the assumption of isotropy will result in predictions that the fabric deforms into a cone when impacted by a projectile. This is different from the pyramidal deformation observed in ballistic tests. The other extreme of fabric modelling that has been reported is to use finite element analysis by discretizing individual yarns into solid elements [5,6]. In the work of Shockey et al. [5], individual yarns were modelled using eight elements over the yarn cross-section and 12 elements along the length within one wavelength of the crimped yarns. Other than yarn crimp, many other features can be incorporated into such a model. However, the model is computationally expensive because of the large number of degrees of freedom involved.

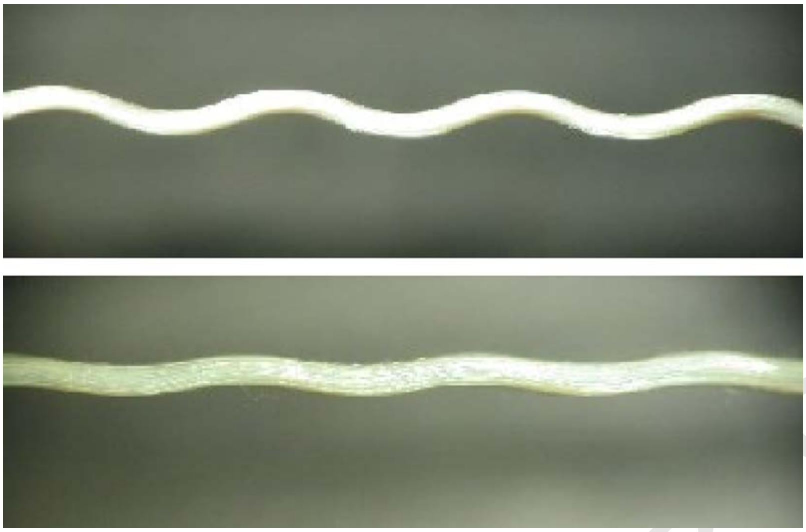

Fig. 1. Crimp in warp (upper) and weft (lower) yarns from CT716 fabric.

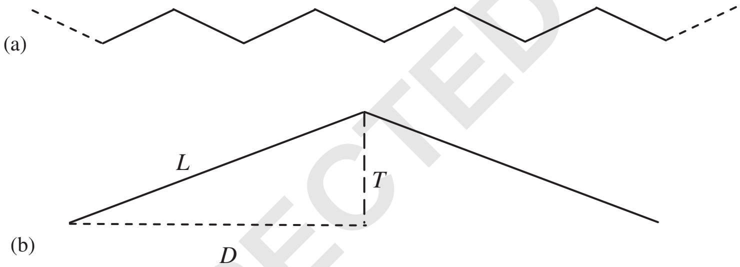

Fig. 2. (a) Idealization of a crimped yarn, (b) crimp parameters.

Another common way to model woven fabric is to idealize it as a network of pin-jointed one-dimensional elements as described by Ting et al. [7], Shim et al. [8] and Tan et al. [9]. Such models are computationally less demanding but sacrifice some details as a result. Nevertheless, important details are retained. For example, the in-plane orthotropy of the fabric is naturally represented and the geometrical and material properties of yarns can be easily incorporated into the one-dimensional elements. The models were found to reflect ballistic impact events observed in actual tests and were able to predict the energy absorbed by fabric very well. In this investigation, such models are adopted to study the effects of these two ways of incorporating crimp.

Plain woven fabric is modelled as nodal masses interconnected by extensible linear fibre elements. The nodal positions and velocities are updated through a finite difference time integration scheme. A three-element viscoelastic constitutive model was proposed to model the response of the polymeric yarns. Written in finite difference form, the nodal velocity at time $t + \Delta t$ is computed from

$$\vec{V}_{t+\Delta t} = \vec{V}_t + \frac{\Delta t}{m}\sum \vec{F}_p, \tag{1}$$

where $\sum \vec{F}_p$ is the resultant force acting on the node arising from tension in the yarn elements connected to it and m is the mass of the node. The nodal positions are then updated using $\vec{V}_{t+\Delta t}$,

$$\vec{X}_{t+\Delta t} = \vec{X}_t + \vec{V}_{t+\Delta t}\,\Delta t. \tag{2}$$

The force $\vec{F}_p$ is computed via a viscoelastic constitutive equation,

$$\vec{F}_{t+\Delta t} = \vec{f}\left(\vec{\sigma}_t, \vec{\varepsilon}_t, \vec{\varepsilon}_{t+\Delta t}\right), \tag{3}$$

where the stress and strain (σ, ε) are calculated for each yarn element linking adjacent nodes.

3.1. Constitutive equations

The constitutive relation for each yarn element is assumed to follow a Zener three-element viscoelastic model, as shown in Fig. 3 [4,8]. The constitutive relationship is described by

$$\left(1 + \frac{K_2}{K_1}\right)\sigma + \frac{\mu}{K_1}\dot{\sigma} = K_2\varepsilon + \mu\dot{\varepsilon}, \tag{4}$$

where σ, ε and $\dot{\varepsilon}$ are the stress, strain and strain rate, respectively. The constants defining the springs (K_1, K_2) and dashpot (μ) are obtained semi-empirically. At a constant strain rate, i.e. $\dot{\varepsilon}(t) = \mathrm{d}\varepsilon(t)/\mathrm{d}t = \dot{\varepsilon}_0$, with initial conditions $\varepsilon = 0$ and $\sigma = 0$, the stress, as a function of strain and strain rate, can be derived from Eq. (4).

$$\sigma = \frac{K_1K_2}{K_1+K_2}\,\varepsilon - \frac{K_1^2\mu}{(K_1+K_2)^2}\,\dot{\varepsilon}_0\left[\exp\left[-\left(\frac{K_1+K_2}{\mu}\right)\frac{\varepsilon}{\dot{\varepsilon}_0}\right] - 1\right], \tag{5}$$

and

$$\frac{\mathrm{d}\sigma}{\mathrm{d}\varepsilon} = \frac{K_1K_2}{K_1+K_2} + \frac{K_1^2}{K_1+K_2}\left[\exp\left(-\left(\frac{K_1+K_2}{\mu}\right)\frac{\varepsilon}{\dot{\varepsilon}_0}\right)\right]. \tag{6}$$

Dynamic tests on Twaron® CT yarns show that their modulus of elasticity increases when the strain rate is increased. The Young's moduli at four strain rates are shown in Table 2 [10]. By correlating these experimental data with Eq. (6), the following values for the parameters were found to give the best fit to test data for a strain of 0.01%; $K_1 = 7.28 \times 10^{10}$ Pa, $K_2 = 4.17 \times 10^{11}$ Pa and $\mu = 6.26 \times 10^8$ Pas.

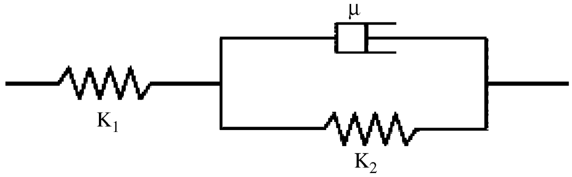

Fig. 3. Zener viscoelastic model.

Table 2
Young's modulus vs. strain rate for Twaron® fiber [8]

Strain rate (s^{-1})	0.01	180	480	1000
E (GPa)	62	69	70	72

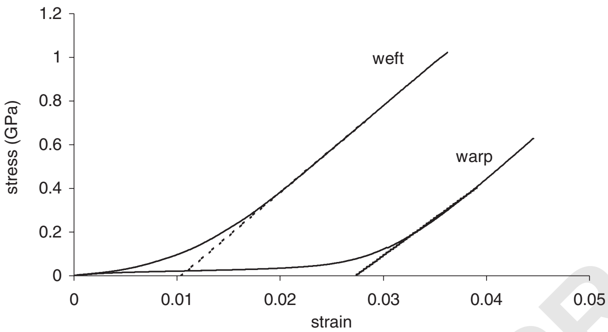

Fig. 4. Uniaxial tensile experimental stress–strain curves for fabric strips in warp and weft directions.

In order to carry out simulations to the point of projectile perforation, it is necessary to define a failure strain for the yarn elements. Quasi-static tests on CT716 yarns gave a failure strain of $\varepsilon_f(\text{static}) = 4.4\%$.

3.2. Modelling crimp

Crimp is a structural artefact that can be accommodated in the network models described by positioning the nodes along the undulating yarns. In this paper, we investigate the feasibility of incorporating crimp into these models by embedding the effects of crimp into the constitutive equation of the yarns.

Simulation results from embedding the effects of crimp into the constitutive equation are compared with those from a model which accounts for crimp structurally by arranging the interconnected elements defining each yarn in a zigzag manner. Computational simulations based on these two different ways of incorporating yarn crimp into the fabric model are also compared with results from actual ballistic experiments on fabric targets.

The advantage of modelling fabric by a planar network of straight yarn elements instead of a network of zigzag yarns elements is that construction of the fabric model becomes simpler. When yarn elements are placed in a zigzag fashion, the normal to the plane of the fabric at each node needs to be computed to determine the start and end points of the yarn elements. Some additional bookkeeping must also be done to track which end of each yarn segment lies above and which lies below the plane of the fabric. The ability to model woven fabric with a planar network overcomes such needs and thus makes the modelling of multiply systems simpler.

The results of quasi-static tensile tests on strips of CT716 fabric are shown in Fig. 4. The fabric strip specimens had a gauge length of 25 mm and were stretched at 5 mm/min. The toe regions in the stress–strain curve are attributed to the straightening out of crimped yarns. The slack in the crimped yarns is estimated to account for strains of 0.0273 in the weft direction and 0.0104 in the warp direction by the time the yarns have straightened out. This means that fabric strain (i.e. strain in the plane of the fabric) is greater than the strain of the yarns until the yarns have straightened out. The relationship between yarn strain and fabric strain is closely approximated by [8].

$$\varepsilon_{\text{yarn}} = \varepsilon_{\text{fabric}} - \varepsilon_{\text{crimp}}(1 - e^{-\varepsilon_{\text{fabric}}/\varepsilon_{\text{crimp}}}), \tag{7}$$

where $\varepsilon_{\text{crimp}} = 0.0273$ for warp direction and 0.0104 for weft direction.

Since Eq. (7) relates strains in the plane of the fabric to strains in the yarns, the nodes and elements of the network model can all be positioned on the plane of the fabric without following the undulations of the crimped yarns. To incorporate crimp into the constitutive equation of the yarns, Eq. (7) is used to convert in-plane strains to yarn strains before Eq. (4) is applied.

4. Ballistic tests

Ballistic tests were conducted on individual plies of Twaron® CT716 fabric specimens measuring 120 mm × 120 mm. Two opposite edges parallel to the warp yarns were fully clamped, i.e. the ends of all weft yarns were clamped, while the ends of all warp yarns were free. The fabric target was subjected to normal impact by a 12 mm spherical projectile weighing 7 g. Tests and simulations were carried out for different projectile striking velocities. The test setup is described by Tan et al. [11]. Impact velocities and residual velocities after perforation by the projectile were recorded, from which the energy absorbed by fabric was obtained. High-speed photography was employed to record the entire process of ballistic impact, which ranged from 10 to 1000 μs.

During ballistic tests, the fabric experienced very high levels of tension, causing the clamped edges to slip. This is especially probable at impact velocities near the ballistic limit. It has been found that slippage is a significant cause of energy dissipation. In order to keep the experiments consistent, only tests with less than 5 mm of slippage were accepted.

5. Energy absorption characteristics

The energy absorbed by the fabric goes into strain energy via the stretching of yarns and kinetic energy of the fabric due to transverse deflection of the fabric and movement of material towards the impact point. It has been established in previous studies that the energy absorbed by fabric exhibits two distinct regimes beyond the ballistic limits—a low-velocity perforation regime and a high-velocity perforation regime [8,11]. Plots of energy absorption against impact velocity obtained from impact tests and from computational simulations using the two different approaches to account for crimp are shown in Fig. 5(a). Transition from the low-velocity regime to the high-velocity regime is marked by a sharp drop in the energy absorbed by the fabric at the critical velocity of 250 m/s. This transition arises when the impact velocity is high enough for the projectile to perforate the fabric even before material distant from the impact point starts to deflect. This results in a sudden drop in energy transferred to the target.

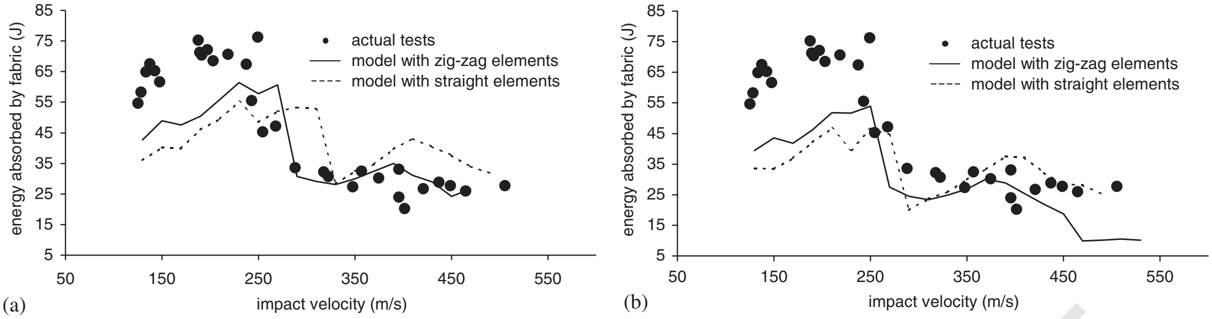

Fig. 5. Measured and predicted values of energy absorbed by CT716 fabric. Prediction with yarn failure strains of (a) 4.4% and (b) 4.0%.

As seen from Fig. 5(a), both fabric models give energy absorption trends consistent with experimental results. There is a continuous increase in energy absorbed until the impact velocity reaches the critical velocity, after which the energy absorbed drops sharply. The numerical simulations are able to predict the critical velocity. However, within the low-velocity regime, the simulation underestimates the energy absorbed by the fabric. The model representing crimp structurally predicts a higher absorbed energy than the model with crimp effects embedded in the constitutive equations. The difference in energy is between 10 and 17 J. This accounts for over 30% of the absorbed energy predicted by the numerical simulations. Accounting for crimp via zigzag elements gives a better prediction of energy absorbed in the low-impact velocity regime. However, in the high-velocity regime, the different methods of incorporating yarn crimp give similar predictions. At high impact velocities, a large part of the fabric is still unperturbed when it is perforated and hence, the results are less sensitive to the way crimp is incorporated into the fabric model. The graphs of energy absorbed against impact velocity from both methods show slight fluctuations but are otherwise consistent with experimental data.

Fig. 5(a) shows results corresponding to use of the static yarn failure strain of 4.4% as a failure criterion for yarn elements. The results for a failure strain of 4.0% are shown in Fig. 5(b). Fig. 5(b) is included to give an indication of the effects of employing a failure strain lower than the static value, which can be expected when polymeric yarns are loaded at high strain rates. Although the lower failure strain leads to a reduction in the energy absorbed by the fabric models, the models continue to give good predictions of the critical velocity and energy absorption for high-velocity impacts.

Fig. 6 shows fabric strain and kinetic energy histories, from impact to perforation, to determine if the two different ways of incorporating crimp would result in significant differences. Numerical results for two impact velocities of 210 and 380 m/s were chosen to study their effects for impacts within the low-and high-velocity regimes. It is observed that both methods of modelling yarn crimp give almost identical predictions of the way fabric strain and kinetic energies increase during impact. Both methods also predict a similar time to perforation and show a larger proportion of energy dissipated as fabric kinetic energy than as strain energy.

The numerical model with zigzag yarn elements gives rise to a marginally lower strain energy and higher kinetic energy compared to the model with straight yarn elements because zigzag yarn

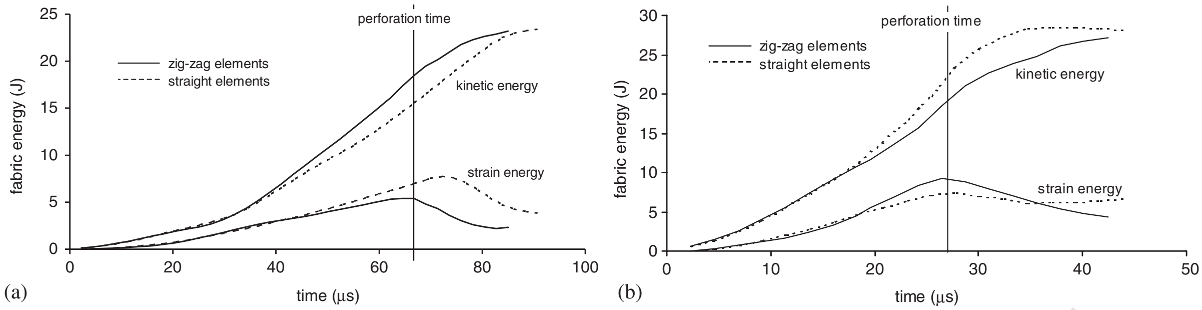

Fig. 6. Fabric strain and kinetic energy histories for impact at (a) 210 m/s and (b) 380 m/s.

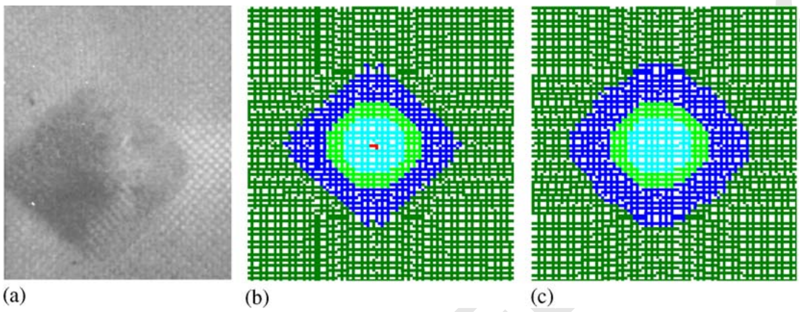

Fig. 7. Fabric deformation around point of impact at 42 μs, (a) actual fabric; (b) model with zigzag yarn elements and (c) model incorporating crimp in constitutive relation.

elements can move more easily but there is less yarn stretching involved. For high impact velocities only a slight difference appears in both strain energy and kinetic energy, as shown in Fig. 6(b).

6. Fabric deformation

Deformation of the fabric during projectile impact is also used to gauge the validity of the fabric models. Figs. 7 and 8 show images of fabric specimens captured by a high-speed camera during impact tests. The images show two obvious features:–

- The fabric deforms into a pyramid with a rhombic base centred at the point of impact.
- The base of the pyramid is elongated towards the clamped edges.

When the projectile strikes the fabric, the impacted region is pushed out of the fabric plane. The primary yarns (yarns in direct contact with the projectile) at the impact point are stretched and tensile waves travel down the primary yarns at the elastic wave speed. Transverse deflection propagates down the yarns in the wake of the elastic wave. The elastic waves and the transverse deflection cannot travel radially away from the impact point because of the nature of the cross-weave. Instead, they travel along the orthogonal directions of the yarns. This gives rise to the

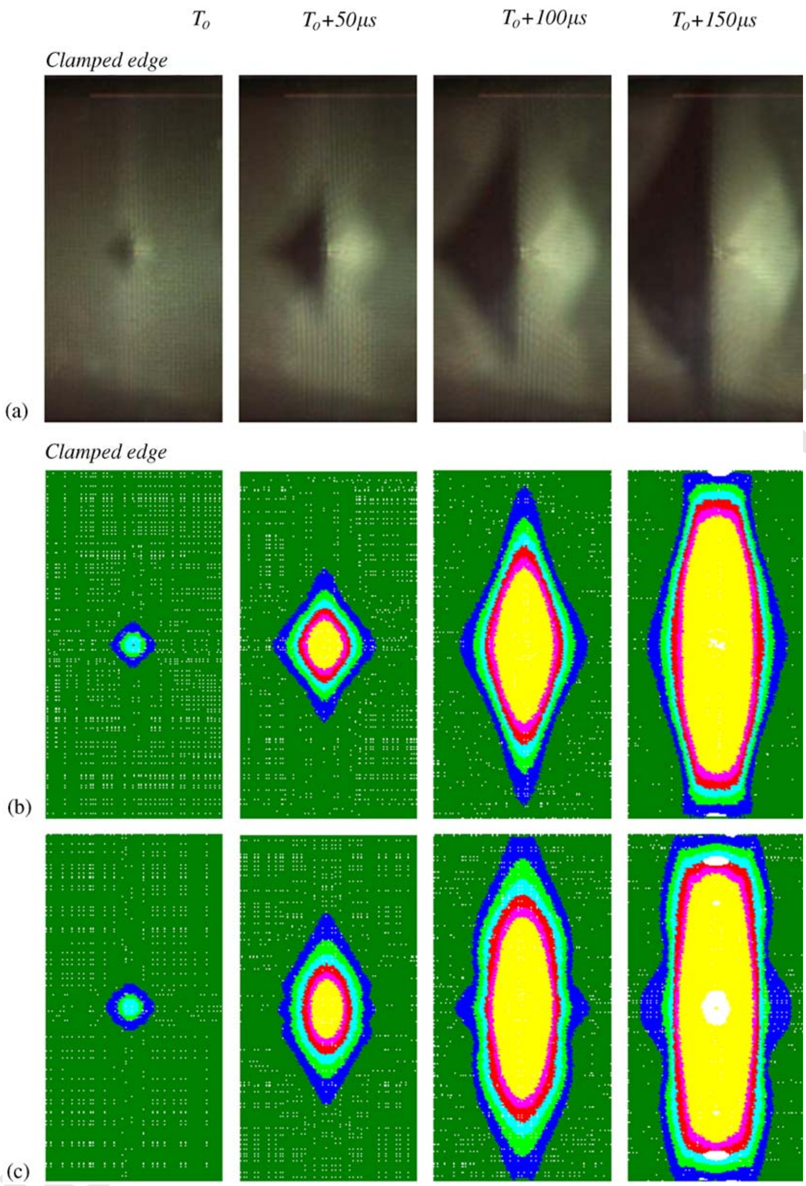

Fig. 8. Fabric deformation for impact at 188 m/s. (a) actual test fabric, (b) model with zigzag yarn elements and (c) model incorporating crimp in constitutive relation. (*material near the free edges is not deflected and is not shown*).

observed pyramidal deformation. The base of the pyramid is elongated in the direction of the clamped yarns because the higher levels of tension in the clamped yarns compared to the free yarns cause the deflection to propagate faster along the clamped yarns.

The deflection predicted from simulations that incorporate crimp via zigzag yarn elements or through constitutive equations reproduces the two main features observed in impact tests during the initial stages of the impact process (Fig. 7). However, as the deflection propagates away from the impact point, the deformed shapes predicted by the two methods start to deviate. Fig. 8(a) shows high-speed images of a fabric deforming when struck by a projectile at 188 m/s. Figs. 8(b) and (c) are images of the deformed fabric predicted by the numerical model using the two different methods to account for crimp as described in Section 3. The computer images and high-speed photographs are all captured at 50 μs time intervals and are scaled to the same size for comparison.

It can be seen from Figs. 7 and 8 that the model which accounts for crimp structurally gives a better prediction of the fabric deformation than the model which accounts for crimp through the constitutive relation of the yarn elements. Fig. 7(b) shows that when yarn elements are arranged in a zigzag manner, the edges of the boundaries of the deflected region are straight, which is similar to actual fabric deformation, whereas the model with straight yarn elements using modified constitutive equations to account for crimp gives rise to an area of deflection that is slightly convex. Fig. 8 also shows that the edges of the deformed area remain relatively straight in actual tests and for the model which accounts for crimp structurally. The second method for accounting for crimp manages to reproduce the general geometry of the deflected fabric region but the deflected area tends to become elliptical and rectangular at the later stages of the impact. Although the outermost fringes are different in Figs. 8(b) and (c), it should be noted that the innermost fringes which represent most of the fabric deformation are similar to one another. Hence, the model with straight yarns may not give as good a prediction as the one with zigzag yarns, but a good approximation of the deformed shape is still obtained.

The speed of the transverse deflection wave front was estimated from the high-speed photographs and compared with numerical simulations. The transverse wave speeds from the zigzag yarn model are closer to the actual ones than the constitutive crimp model. The predicted transverse deflection wave speed from numerical computation is always higher than the actual wave speed along clamped yarns. Once the transverse deflection wave front reaches the clamped boundary, yarns are fully stretched and any further stretching will quickly lead to perforation. In Fig. 8, the structural crimp model starts to fail only at $T_o + 150\,\mu s$ while the constitutive crimp model has already been perforated. At this time, the transverse deflection of the actual fabric has not reached the clamped edges. The higher than actual wave propagation speed in the numerical model could be the cause of the underestimation of the energy absorbed by the fabric (Fig. 5) in the low-impact velocity regime. This effect may not be significant in the high-impact velocity regime because the fabric is perforated before the deflection propagates to the edges.

When woven fabrics are stretched in one of the yarn directions, yarns in direction of the load straighten while yarns in the orthogonal direction become more crimped. Therefore, the fabric stretches in the direction of the load and shrinks perpendicular to it, giving rise to a 'Poisson's' effect. A shortcoming of incorporating the effects of crimp in the constitutive relationship is that this 'Poisson's' effect is not represented. This effect shows up in the deformation of the fabric models. When the clamped yarns straighten during impact and the unclamped yarns become more crimped in the model with the zigzag yarns, propagation of deflection along the unclamped yarns is further delayed because the unclamped yarns need to straighten some more before they undergo tension and start pulling neighbouring yarn elements. Hence, for yarns not in direct contact with the projectile, the propagation of yarn deflection is slower in the model with zigzag yarns than the model with straight yarns. This effect is observed in the larger and more elliptical shape of the deformed area for the model with straight yarns, as seen in Fig. 8.

7. Inter-yarn friction

It has been reported that increasing inter-yarn friction improves the ballistic resistance of woven fabrics [12–15]. With higher friction, it becomes more difficult for a projectile to push yarns apart and hence, they have to engage and break more yarns in order to perforate the fabric. Because friction between yarns is determined by the manner in which yarns contact one another, it becomes important to model the undulations in crimped yarns in order to allow for yarns to slide against one another. While the current models do not cater for yarn slippage, the forces at crossover points can be computed to give an indication of frictional forces required to keep the yarns from slipping. The normal and tangential forces at all crossover nodes were monitored and the ratio of the two calculated. Fig. 9 shows contour plots of the ratio of the tangential to the normal force in the fabric at crossover points for the model with zigzag yarn elements and the model with straight yarns. This gives direct information on the tendency of slippage between yarns at crossover points. It was found that slippage is very likely to occur at crossover points along primary yarns and near the unclamped edges. The fibre-to-fibre friction coefficients for aramid were reported to be 0.22 at a sliding speed of 9.6 mm/min and 0.27 at a sliding speed of 77×10^3 mm/min [16]. High stress levels in primary yarn elements are expected to trigger slippage.

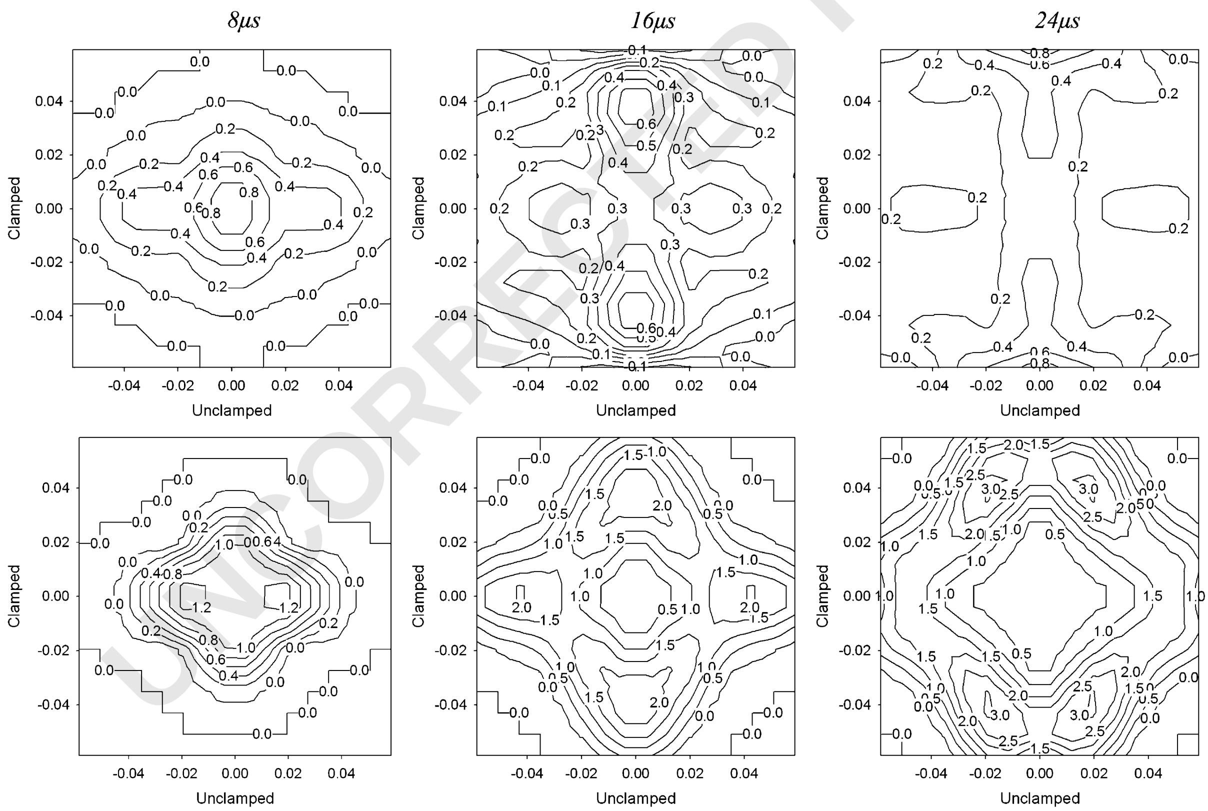

Fig. 9. Ratio of tangential force to normal force at yarn crossover points for an impact velocity of 400 m/s: (a) model with zigzag yarn elements and (b) model with straight yarn elements.

It is observed that the ratio predicted by the model with straight yarns is much higher and the tendency to slip is more widespread within the fabric target compared with that from the model with zigzag yarn elements because the normal component of the inter-yarn forces is lower for straight yarn elements.

8. Conclusions

Cross-woven fabric armour was modelled as a network of pin-jointed one-dimensional elements with viscoelastic properties. Yarn crimp (undulations in the yarns due to weaving) can be incorporated into the model by either arranging the yarn elements in a zigzag manner to accurately reflect the structure of the fabric or by leaving the yarn elements straight but discounting some element strain that arises from straightening of the yarns via the constitutive equations of the elements. A comparison of the simulation results with actual ballistic tests shows that while the model with zigzag yarn elements gives results that are in closer agreement with actual tests, the difference between the two methods of incorporating crimp is marginal in terms of predicting energy absorption characteristics and fabric deformation.

The model with zigzag yarn elements gives slightly closer quantitative agreement with experimental results than the model with straight yarn elements. The main difference is that the first model is able to reproduce the observed deformation throughout the entire impact process up to the point of perforation, whereas the fabric deformation predicted by the second model starts to deviate from actual test results as impact progresses. This also results in a slightly lower prediction of the energy absorbed at low-impact velocities by the model with straight yarn elements. Both models gave good predictions of the energy absorbed by the fabric at high-impact velocities and showed similar strain and kinetic energies for low- and high-velocity impacts. The biggest difference between the two models is the ratio of the tangential to the normal force between the yarns. The model with straight elements showed a much larger tendency for inter-yarn sliding compared to the model with zigzag elements.

9. Uncited reference

[17].

Reference

[1] Cheeseman BA, Bogetti TA. Ballistic impact into fabric and compliant composite laminates. Compos Struct 2003;61:161–73.
[2] Chitrangad. Hybrid ballistic fabric. United States Patent No.5,187,003, 16 February 1993.
[3] Taylor Jr. WJ, Vinson JR. Modeling ballistic impact into flexible materials. AIAA J 1990;28:273–93.
[4] Lim CT, Shim VPW, Ng YH. Finite-element modeling of the ballistic impact of fabric armor. Int J Impact Eng 2003;V28(1):13–31.
[5] Shockey DA, Erlich DC, Simons JW. Lightweight fragment barriers for commercial aircraft. In: 18th international symposium on ballistics, US, 1999.

[6] Duan Y, Keefe M, Bogetti TA, Cheeseman BA. Modeling the role of friction during ballistic impact of a high-strength plain-weave fabric. Compos Struct [article in press].
[7] Ting C, Ting J, Cunniff P, Roylance D. Numerical characterization of the effects of transverse yarn interaction on textile ballistic response. In: 30th International SAMPE technical conference, October 1998.
[8] Shim VPW, Tan VBC, Tay TE. Modeling deformation and damage characteristics of woven fabric under small projectile impact. Int J Impact Eng 1995;6(4):585–605.
[9] Tan VBC, Shim VPW, Tay TE. Experimental and numerical study of the response of flexible laminates to impact loading. Int J Solids Struct 2003;40:6245–66.
[10] Gu B. Analytical modeling for the ballistic perforation of planar plain-woven fabric target by projectile. Composites: Part B 2003;34:361–71.
[11] Tan VBC, Lim CT, Cheong CH. Perforation of high-strength fabric by projectiles of different geometry. Int J Impact Eng 2003;28:207–22.
[12] Lavielle L. Polymer-polymer friction—relation to adhesion. Wear 1991;151:63–75.
[13] Briscoe BJ, Motamedi F. The ballistic impact characteristics of aramid fabrics: the influence of interface friction. Wear 1992;158:229–47.
[14] Briscoe BJ, Motamedi F. Role of interfacial friction and lubrication in yarn and fabric mechanics. Text Res J 1990;60:697–708.
[15] Prosser RA. Penetration of nylon ballistic panels by fragment-simulating projectiles, Part2: mechanism of penetration. Text Res J 1988.
[16] Rebouillat S. Tribological properties of woven para-aramid fabrics and their constituent yarns. J Mater Sci 1998;33:3293–301.
[17] Roylance D, Wang SS. Penetration mechanics of textile structures. In: Laible RC, editor. Ballistic materials and penetration mechanics. Amsterdam: Elsevier; 1980.